

ABLATION OF CARBON-BASED MATERIALS: MULTISCALE ROUGHNESS MODELLING

Gerard L. Vignoles¹, Jean Lachaud¹, Yvan Aspa^{1,2}

¹ Laboratoire des Composites ThermoStructuraux (LCTS) - UMR 5801 Univ. Bordeaux 1-CNRS-SNECMA-CEA - 3, Allée La Boétie, Domaine Universitaire, Pessac, F33600 France

² Institut de Mécanique des Fluides de Toulouse (IMFT) - UMR 5502 INPT-CNRS - 1, Allée du Professeur Camille Soula, Toulouse, F 31000 France

ABSTRACT

Various kinds of carbon-based materials are used for the thermal protection of systems at extreme temperatures, like atmospheric re-entry shields and rocket nozzles, because of their unique ablative properties. A critical issue in the design of such systems is the knowledge of the surface roughness evolution.

This work deals with ablation, either by oxidation or by sublimation, from the material point of view. First, various features and scales of roughness morphology are presented, and a tentative classification is proposed. Then, a modelling strategy based on the competition between transfer at the material interface and in the overlying bulk phase, with possible reactivity contrasts between the material constituents, is built.

Numerical results at various scales are given. Some predicted morphologies are in correct agreement with the experimental observations. A parameter variation study shows that the morphological features are dictated by the reactivity contrast of the material components, and on diffusion/reaction competitions.

This allows to identify physico-chemical parameters from the roughness geometry, as in an inverse method.

1. INTRODUCTION

Ablative Thermal Protection Systems (TPS) are the most traditional materials for atmospheric re-entry nose-tip protection; among them, carbon/carbon (C/C) and carbon/phenolic resin (C/R) composites are of common use [1,2], because of their excellent compromise between thermal, thermo-chemical and mechanical properties [3]. The principle of thermal protection is that an appreciable amount of the received heat flux is converted into outwards mass flux through endothermic sublimation and chemical etching: this induces surface recession [4]. Surface roughening then appears: this banal but uncontrolled phenomenon has several consequences of importance in the case of atmospheric re-entry. First, it increases the chemically active surface of the wall; and second, it contributes to the laminar-to-turbulent transition in the surrounding flow [5,6]. Both modifications to the physico-chemistry lead to an increase in heat transfer, resulting in an acceleration of the surface recession [7]. The TPS thickness design has to account for this rather strong effect.

Another spatial application for the same class of materials is the fabrication of rocket nozzle throats and inner parts. Here again, the acquisition of surface roughness during rocket launch is a critical issue, not because of the laminar-to-turbulent transition, but principally because of its impact on surface recession velocity, and on the possibility of triggering mechanical erosion [8].

For both applications, if general phenomenological tendencies are predictable, the understanding of the interaction between the flow and the material has to be improved. In this work, an effort is done to improve this comprehension through the observation, the

study and the modelling of roughness evolution, focusing on the primary cause which is heterogeneous transfer. This document features three parts: First, a description and a classification of multi-scale surface roughness features appearing on carbon-based materials are proposed. Then, physico-chemical models are set up to explain the formation of the typical roughness patterns. Numerical and analytical results are finally presented and discussed with respect to the experimental observations.

2. ROUGHNESS OBSERVATION AND CLASSIFICATION

The studied materials are :

- (1) A 3D C/C composite, made from a 3D ex-PAN carbon fibre preform and a pitch-based carbon matrix. It is a heterogeneous multi-scale material. Several thousands of fibers are linked together into a unidirectional bundle with a pitch-based matrix (mesostructure). Then, bundles are orthogonally fit together into a pattern repeated by translation on a cubic lattice. This macro-structure leads to a network of parallelepipedic macro-pores (located near each node of the lattice), which are partially filled with pitch matrix.
- (2) A pyrolysed C/phenolic resin composite, made from ex-cellulose fibres grouped in bundles, which are themselves woven in satin plies; the plies are then stacked together and impregnated with phenolic resin. Under typical ablation conditions, the phenolic resin is not any more present as such, but has suffered pyrolysis and is transformed into a highly porous carbon with an approximate density of 700 kg.m^{-3} .
- (3) Polycrystalline graphite samples, with an approximate grain size of $5 \text{ }\mu\text{m}$. The grains are joined together by a less organised carbon obtained by pyrolysis of pitch.

Unfortunately, it is quite difficult to recover samples from real flight experiments. As far as roughness is concerned, arc-jet ground tests are supposed to be representative of real flight conditions [9]. The samples have been submitted to arc-jet tests in stagnation point configuration. In this case, the material temperature is high enough (3000 K) to enable both oxidation and sublimation. Other tests have been performed in an atmospheric pressure oxidation reactor, with temperatures ranging from 600 K to 900 K.

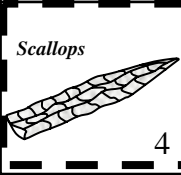
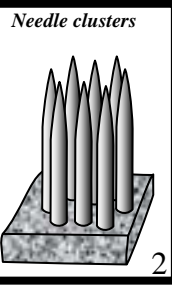
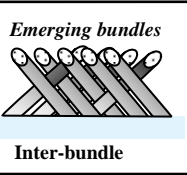
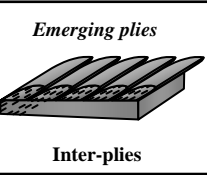
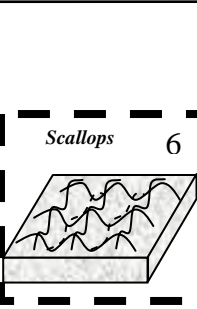
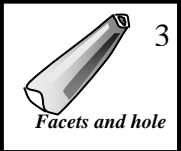
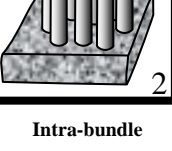
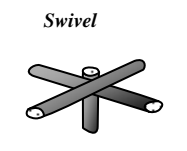
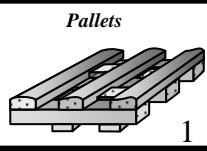
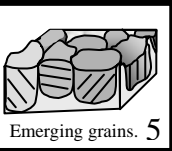
Surface roughness has been observed by binocular magnifier (BM), optical microscope (OM), scanning electron microscopy (SEM), laser profilometry and X-ray Computed Microtomography (CMT). A classification of the observed roughness features according to their length scales is presented on Table 1. Several characteristic features are illustrated at figs. 1 to 6. The morphological patterns may be organised following two criteria: (1) the presence or absence of an underlying material heterogeneity, and (2) the characteristic length scale. Ablation features supported by the material heterogeneity will be called “structural roughness”, while in the converse case we will refer to “physical roughness”. Structural roughness is the easiest to understand and describe. According to the characteristic length, it is possible to distinguish :

- (1) Epimacrostructural roughness takes place on the lattice. It seems to result from the difference of reactivity between bundles and extra-bundle pitch-based matrix. Mechanical erosion sporadically occurs through the detachment of an extra-bundle matrix octet. The section of emerging bundles (tangent or perpendicular to surface) is slightly undulating. Indeed, if edges of initially square section of bundles are emerging, creating crenels, they are smoothed out to a wavy form by ablation. An OM micrograph of a polished slice, presented on Fig. 1, associated to the knowledge of the material structure, enable us to sketch the "pallet" scheme.

(2) Epimesostructural roughness develops at the top of emerging bundles, and looks like "needle clusters" (resp. "needle layers") for bundles perpendicular (resp. parallel) to material surface. In the literature, many micrographs show such roughness features on carbon-based composites during ablation by oxidation [10, 11] or both oxidation and sublimation. [12-14] As shown on fig. 2, due to an important recession of the intra-bundle matrix, fibers, which are less reactive, are partially stripped, become thinner, and acquire a needle shape.

(3) Epimicrostructural roughness appears on the microstructure. Fiber tips are faceted (Fig. 3). Some materials also show holes on the top of the fibers. In the same category, one finds the grain-supported roughness of polycrystalline graphite, as illustrated at Fig. 5.

Tab. 1. Classification of roughness morphologies. The black boxes correspond to photographs of figs. 1-6. Continuous line borders refer to structural roughness and dashed line borders refer to physical roughness.

Roughness Scale	MICRO-SCALE		MESO-SCALE		
Material scale	microstructure		mesostructure		composite
	fibre / grain	bundle	Weave pattern	Plies	REV
	micrometre		millimetre		centimetre
C/phen	 4	 2	 Inter-bundle	 Inter-ply	 6
C/C	 3	 2	 Swivel	 1	
Polycr. Graphite		 5			

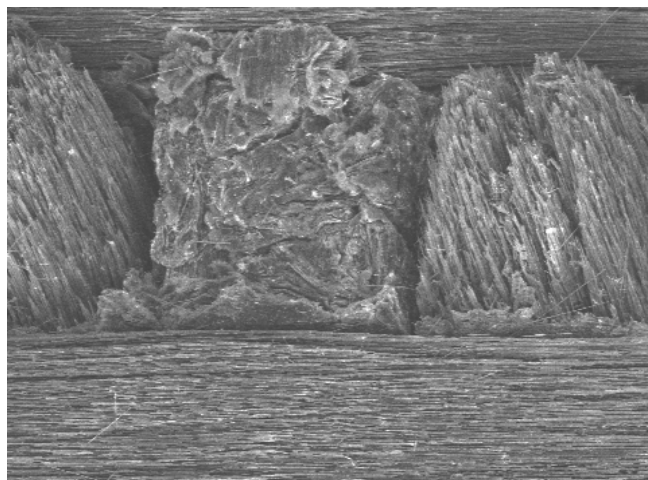


Fig. 1. Optical Micrograph of a 3D C/C ablated composite.

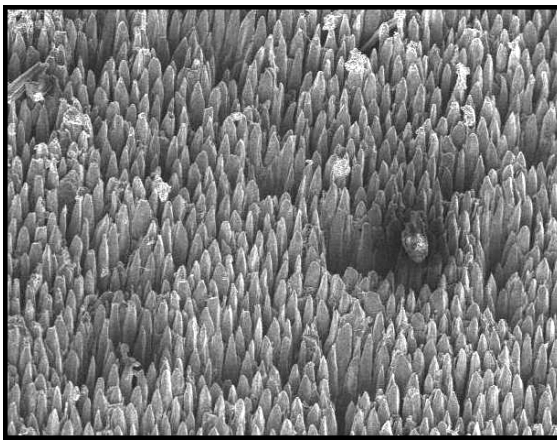


Fig. 2. SEM image of a “fibre forest”, in an emerging bundle of a 3D C/C composite.

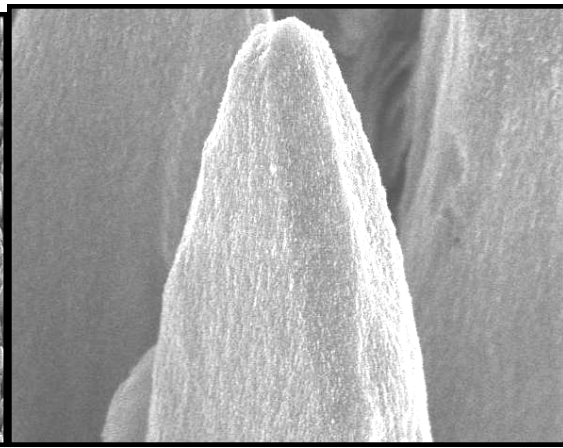


Fig. 3. SEM image of an ex-PAN fibre tip displaying facets (3D C/C composite).

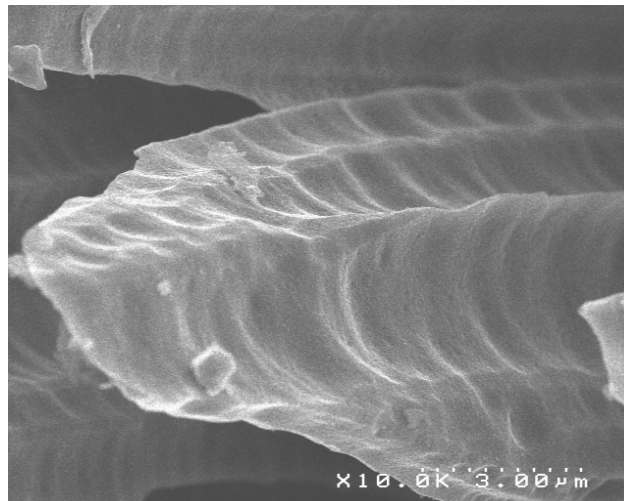


Fig. 4. SEM image of an ex-cellulose fibre tip displaying scallops (2D C/R composite).

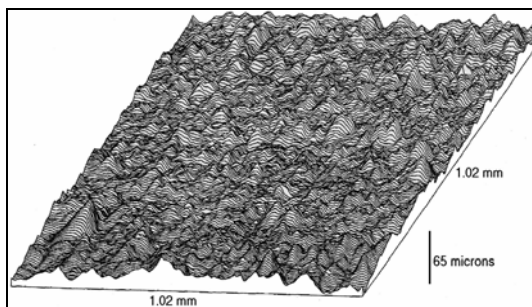


Fig. 5. Profilometric graph of a polycrystalline graphite sample ablated in laminar flow regime.

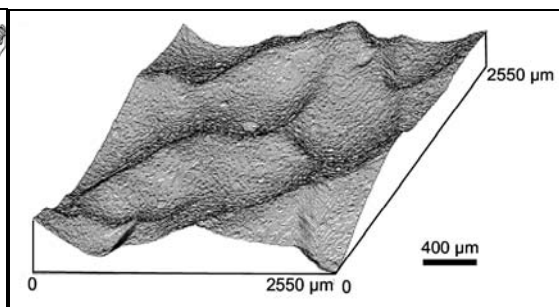


Fig. 6. Profilometric graph of a polycrystalline graphite sample ablated in turbulent flow regime.

The second kind of roughness features is identified on materials or material components which do not display evidence of local heterogeneity. It consists in “scallops” or “thumbprints”, which are similar to the “regmaglypts” observed on meteorites. These have been long ago described on materials which have suffered ablation tests [15,16] and are found again in the present observations, either on a naked fibre tip with micrometer-long scallops (fig. 4) or on a polycrystalline graphite sample ablated in turbulent flow conditions, with millimetre-long features (fig. 6). The fact that two very dis-

tinct length scales exist on similar carbon-base materials will be addressed in the following. Evidently, physical roughness may only arise from transfer phenomena between the solid and the gas phases : this will be accounted for in the modelling strategy presented next.

2. MODELLING PRINCIPLES

From the morphological study presented above, it appears that the modelling of the roughness onset should feature the following elements :

- (i)- Surface recession, under the action of oxidation or of sublimation. The surface recession velocity at any point depends on surface orientation, and on the rate of mass transfer. This latter quantity is a function of surface temperature and of local concentration of reactant gas or the local partial pressure of sublimed species, compared to the equilibrium value, *e.g.* through a Knudsen-Langmuir relationship.
- (ii)- The local gas concentration is attained by solving a mass balance equation featuring consumption or production by the surface, and transport in the bundle of the gas phase.
- (iii)- Similarly, the local surface temperature is evaluated by a heat balance equation featuring transport in the solid gas phases, as well as interfacial heat consumption.
- (iv)- When necessary, the chemical reactivity will be a function of space, in order to translate the possible material heterogeneity.

Point (i) is modelled by a Hamilton-Jacobi equation which describes the propagation of the surface under the action of a Hamiltonian which depends a priori on surface concentration and temperature. Points (ii) and (iii) may be modelled by transport equations for gas species and temperature ; gas-phase transport should feature diffusion (possibly multi-component), and convection. This last element requires knowledge of the gas phase velocity field, in possibly turbulent flow conditions, which may be extremely difficult to obtain in a realistic fashion.

A first model may be built using a set of rather restrictive assumptions :

- Isothermal conditions. This is suited to two kinds of situations : (1) isothermal oxidation tests ; (2) micro-scale simulations where it appears that temperature differences across a characteristic roughness feature length are small enough to be neglected.
- Gas transport is restricted to the pure diffusion of a single species between the surface and a gas source (or sink) located at a large enough distance above the surface ; at this place, it is considered that convection ensures the constancy of gas concentration. The relation between source concentration and source-to-surface distance may be obtained through a boundary-layer analysis. The criterion for the choice of the source-to-surface distance is based on a perturbation analysis argument, which shows that it can be as small as a few times the transverse characteristic length of the roughness pattern.
- Surface gas transfer is first order. It can be shown that oxidation and sublimation follow the same formalism in these conditions [17].

Even though this model looks extremely restrictive, it has the merit of being easily tractable and of capturing the essentials of the bulk transport/interfacial transfer competition. Moreover, it will appear that most of the roughness set-up dynamics is governed by the material itself, which will be correctly described by the model ; on the other hand, there is absolutely no pretension to describe accurately the gas flow.

A second model may be easily built on the basis of the first one, by taking an analogy between heat and mass transfer ; for this, it suffices to replace gas concentration by temperature. This will be adequate for large-scale modelling, where the gas diffusive boundary-layer thickness is very small with respect to the thermal boundary layer.

Results from these two simple models (later on referred to as “Model 1” and “Model 2”) will be presented in the following part.

3. RESULTS

3. 1 - Physical Roughness (Scallops)

The simplest modelling case concerns Model 1 with a chemically homogeneous surface. A mathematical analysis of the diffusion-reaction-recession problem [17] shows that there exist stable steady-state morphologies which are made of circle arcs (or sphere segments in 3D) or flat segments, connected together by symmetrical singular points, as shown at fig. 7.

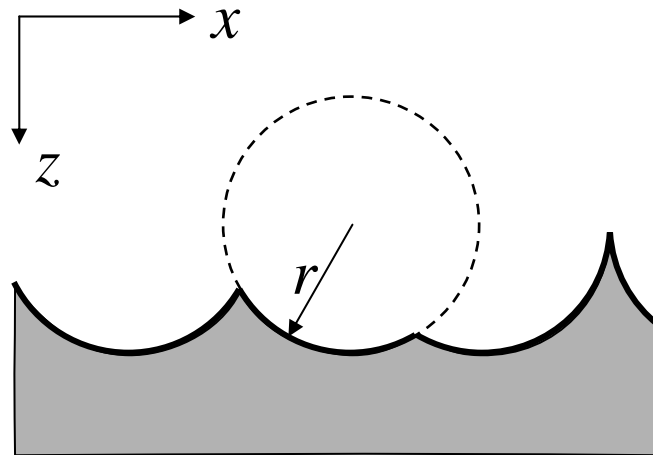


Fig. 7 : Possible 2D steady-state roughness patterns

The curvature radius is simply $r = D/k$ where D is the diffusion coefficient and k is the heterogeneous reaction constant in m.s^{-1} . Estimation of this quantity in the ablation case of fig. 4 (C/R fiber tip) yields a value of the order of $1 \mu\text{m}$, in agreement with the observed scallop curvature radius. Numerical simulations have confirmed the stability of the scalloped surfaces and shown that the transient times are short ($\tau \approx 3 C_0 M_s k^2 / D \rho_s$) [18]. The fact that scallops are obtained results from the growth of initial perturbations, which may have several origins, like local material heterogeneity, turbulence in the flow, or else.

Switching now to model 2, the diffusion coefficient is replaced by the gas thermal diffusivity $a_g = \lambda_g / \rho_g c_{pg}$, and the heterogeneous reaction constant has to be replaced by its temperature-related analogue, *i.e.* [19] :

$$k' = (\Delta_r H / C_{pg} T_0) (E_a / RT_0) k(T_0) \quad (1)$$

where $\Delta_r H$ is the ablation molar enthalpy change, C_{pg} is the gas molar heat capacity, E_a the activation energy of the ablative process, and T_0 a reference surface temperature (for example, at scallop bottom). This gives a new curvature radius expression :

$$r = a/k' = \frac{RT_0}{E_a} \cdot \frac{\lambda T_0}{C_0 \Delta_r H k(T_0)} \quad (2)$$

where C_0 is the bulk gas concentration. A numerical evaluation of this quantity [17,18] gives $r \sim 3$ mm, matching well the situation depicted at Fig. 6. As a conclusion, it is shown that physical roughness indeed results from a bulk transfer/interfacial transfer competition : more elevated surface points are closer to the source, but if they are more inclined, they receive the same flux as point which lie less close but have less inclination : this ensures the steadiness of the surface morphology. A perturbation analysis has confirmed that the scallops are as stable as the flat surface.

3. 2 - Microscale roughness : needle stackings

The next case concerns Model 1 again, with a chemically heterogeneous surface : here, the model system is a moderately reactive fiber surrounded by a more reactive matrix. Again, an analytical study, in an axisymmetric configuration, and with a steady-state hypothesis, has allowed to obtain the equation of the fibres ogival surface. The peak-to-valley roughness is then given by the following formula :

$$\frac{h_f}{r_f} = \left(\frac{La}{r_f}\right) \left(\sqrt{\left(\frac{r_f}{La}\right)^2 + 2\sqrt{A^2-1} \left(\frac{r_f}{La}\right) - 1} - 1 \right), \quad \text{where } A = \frac{k_m M_m \rho_f}{k_f M_f \rho_m} \quad (3)$$

Interestingly, one notes that this quantity is again dictated by a characteristic length $La = D/k_m$ arising, as in the preceding section, from the competition between diffusive bulk transport and the matrix heterogeneous transfer. A matrix-to-fibre contrast ratio A also arises from this study, as could be expected.

Numerical simulations of this problem have been performed independently with two solvers. The first is based on a finite difference scheme for diffusion, a VOF (Volume-Of-Fluid) model for surface recession, and a PLIC (PLanar Interface Construction) discretisation of the interface boundary [20,21]. The second one [22] is based on a Monte-Carlo-Random Walk (MC/RW) algorithm for gas diffusion, with a suited sticking probability low for surface reaction, and a simplified Marching-Cube discretisation of the interface [23]. Both solvers yield equal results : a steady-state morphology in very good agreement with the analytical formula is obtained (see fig. 8) ; moreover, the transient time is of the order of a few time scale units :

$$\tau \sim 3 \frac{\rho_m (\delta_c + h_f)^2}{DC_0 M_m} \quad (4)$$

Note that in certain material conditions, this may be a rather long time. The analytical and numerical studies also allow to assess the equivalent composite recession rate :

$$V_{\text{eff}} = \frac{C_0 k_m M_m}{\rho_m (1 + k_m (h_f + \delta_c) / D)} \quad (5)$$

Eqs (4) and (5) show that the matrix reactivity is the most important control parameter, *i.e.* the weakest phase determines the composite behaviour. Using the combination of eqs (3-5), it is possible to perform a direct assessment of fibre and matrix reactivities from the study of the morphology and recession rate. In the case of fig. 4 (2D C/R) a fibre-to-matrix reactivity ratio of 30 has been found, in correct agreement with independent measurements made on pure fibres and pyrolysed matrix. The case of fig. 3 is presented in [24].

3.3 - Microscale roughness : grain-supported features

The case of polycrystalline graphite may be treated by Model 1, adding as an extra feature a dependence of the reactivity to orientation, which illustrates the anisotropy of graphite. Indeed, graphene edge reactivity is known to be much larger than in the perpendicular direction. The following law for the orientation-dependent reactivity has been chosen :

$$k_{\text{eff}}(\theta) = \frac{k_{//}|\sin \theta| + k_{\perp}|\cos \theta|}{|\sin \theta| + |\cos \theta|} \quad (6)$$

Numerical simulation has been performed with the MC/RW-SMC algorithm, and yields typical morphologies as illustrated at fig. 9 ; comparing with fig. 5 shows that a very good qualitative agreement may be obtained. In this case, the grain-related peak-to-valley roughness is roughly 1/3 of the grain size.

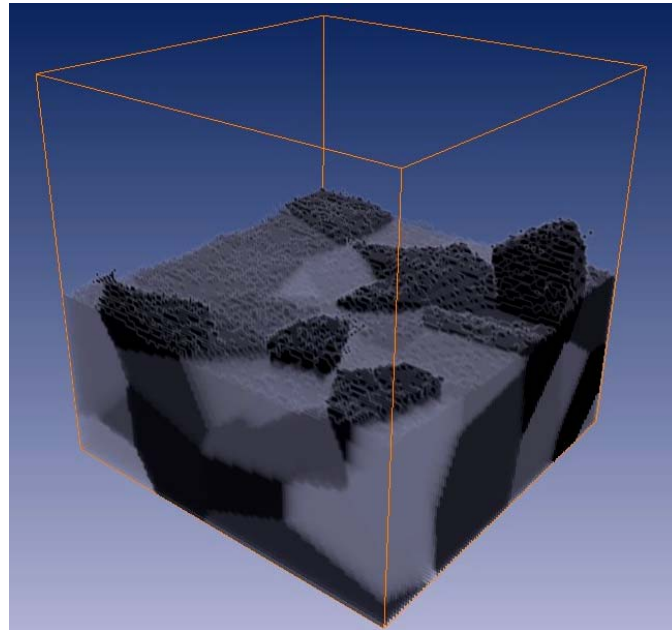


Fig. 9 : Example of roughness morphology simulation for polycrystalline graphite.

4- Macroscale features

The last model case concerns large-scale simulation of epimacrostructural roughness. Here, Model 2 is used, and the model system is a 3D C/C composite with vertical and horizontal bundles of similar but anisotropic reactivity, and a more reactive inter-bundle matrix. The transient time being possibly larger than the total experiment time, no attempt to reach a steady-state morphology is made. The numerical result of fig. 10 shows excellent qualitative agreement with fig. 1. Since the intrinsic reactivity of the constitu-

ents is not known separately, a parameter variation study has been made in order to obtain the agreement, through a kind of inverse-problem analysis. This illustrates the potential of the method in the extraction of material parameters from simple experimental data.

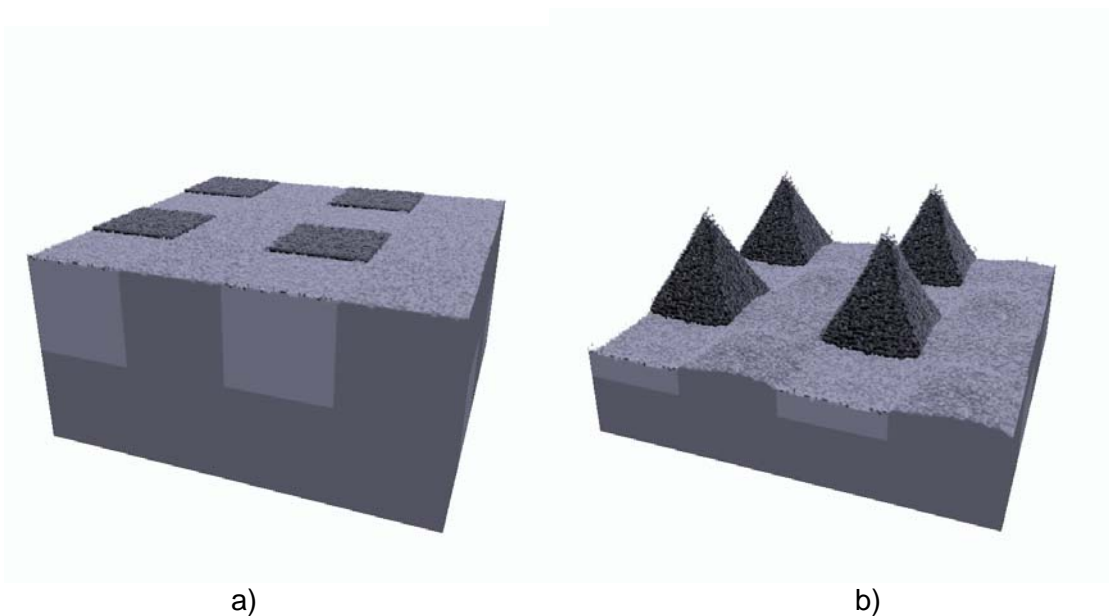


Fig. 9 : 3D composite material macro scale ablation simulations : **a)** at $t = 0$, **b)** at $t = 3\tau$

3. CONCLUSIONS

This work shows that the large diversity of roughness feature morphologies and length scales may be explained and modelled with a rather simple approach based on the competition between bulk transfer and heterogeneous transfer, be it either of gas or of heat. The larger length scales are related to heat transfer, while the smallest are related to mass transfer. Reactivity (or heterogeneous transfer coefficient) differences between constituents are suited to explain structural roughness, while physical roughness (scallop) is explained by the bulk/interfacial transfer competition itself.

Many perspectives arise from these studies. First, more systematic experimental verifications have still to be performed in several situations, in order to confirm the predictive power of the approach. Second, on exploitation in terms of guidelines for material optimization is at hand : it should be possible to use the presented tools to seek for composites with less pronounced roughness and /or equivalent reactivities. Third, the modelling tools have to be improved in several points : simultaneous resolution of heat & mass transfer, coupling with flow computations for the inclusion of convection, multicomponent diffusion, etc These will be the aim of future works.

ACKNOWLEDGEMENTS

The authors acknowledge Snecma Propulsion Solide for a PhD grant to Y. A., and CEA for a grant to J. L.

References

1. **Manocha, L. M.** and **Fitzer, E.**, "Carbon reinforcement and C/C composites". Springer, Berlin (1998).

2. **Duffa, G.**, "Ablation". CEA, Le Barp, France ISBN 2-7272-0207-5 (1996)
3. **Savage, G.**, "Carbon/Carbon Composites". Chapman & Hall, London (1993).
4. **Couzi, J., de Winne, J. and Leroy, B.**, "Improvements in ablation predictions for reentry vehicle nosetip". In *Proc. 3rd Eur. Symp. on Aerothermodynamics for Space Vehicles*, ESA, Noordwijk, The Netherlands (1998), pp. 493-499.
5. **Jackson, M. D.**. "Roughness induced transition on blunt axisymmetric bodies", Interim Report SAMSO-TR-74-86 of Passive Nosetip Technology (PANT) Program n°15 (1974).
6. **Reda, D. C.**. "Correlation of nosetip boundary-layer transition data measured in ballistic-range experiments", Sandia Report SAND 79-0649 (1979).
7. **Batt, R. G. and Legner, H. H.**. "A review of roughness-induced nosetip transition", *AIAA Papers* **21**(1983), 7-22.
8. **Borie, V. , Maisonneuve, Y. , Lambert, D. and Lengellé, G.**. "Ablation des matériaux de tuyères de propulseurs à propergol solide". Technical Report N°13, ONERA, France (1990).
9. **Wool, M. R.**. "Summary of experimental and analytical results", Interim Report SAMSO-TR-74-86 of Passive Nosetip Technology (PANT) Program n°10 (1975).
10. **Cho, D., Lee, J. Y., and Yoon, B. I.**. "Microscopic observations of the ablation behaviours of carbon fibre/phenolic composites". *J. Mater. Sci.* **12** (1993) 1894-1896.
11. **Duvivier, E.**. "Cinétique d'oxydation d'un composite carbone/carbone et influence sur le comportement mécanique". PhD thesis n° 1692, University Bordeaux 1, France (1997).
12. **Cho, D. and Yoon, B. I.**. "Microstructural interpretation of the effect of various matrices on the ablation properties of carbon-fiber-reinforced composites". *Compos. Sci. and Technol.*, **61** (2001) 271-280.
13. **Han, J. C., He, X. D. and Du, S. Y.**. "Oxidation and ablation of 3D carbon-carbon composite at up to 3000 °C". *Carbon* **33** (1995) 473-478.
14. **Lee, Y.-J. and Joo, H.-J.**. "Investigation on ablation behavior of CFRC composites prepared at different pressures". *Composites: Part A* **35** (2004) 1285-1290.
15. **Larson, H. K. and Mateer, G. G.**, "Cross-hatching - A coupling of gas dynamics with the ablation process", *AIAA Paper* **68**-670 (1968).
16. **Williams, E. P.**, "Experimental Studies of Ablation Surface Patterns and Resulting Roll Torques", *AIAA J.* **9** (1971) 1315-1321.
17. **Duffa, G. , Vignoles, G. L., Goyhénèche, J.-M. and Aspa, Y.**. "Ablation of carbon-based materials : investigation of roughness set-up from heterogeneous reactions". *Int. J. Heat and Mass Transfer*, **48** (2005) 3387-3401.
18. **Vignoles, G. L., Goyhénèche, J.-M., Duffa, G., N'guyen-Bui, T.-H., Velghe, A., Dubroca, B. and Aspa, Y.**. "Scalloped morphologies of ablated materials", *Ceram. Eng. Sci. Proc.* **26** (2005) 245-252.
19. **Vignoles, G. L., Lachaud, J. and Aspa, Y.**, "Roughness evolution in ablation of carbon-based materials : multi-scale modelling and material analysis", *Proc. 5th Eur. Workshop on Thermal Protection Systems and Hot Structures*, ESA, Noordwijk, The Netherlands, to appear (2006)
20. **Aspa, Y., Quintard, M., Plazanet, F., Descamps, C. and Vignoles, G. L.**, "Ablation of Carbon/Carbon Composites : Direct Numerical Simulation and Effective Behavior", *Ceram. Eng. Sci. Proc.* **26** (2005) 99-106.
21. **Aspa, Y., Lachaud, J., Vignoles, G. L. and Quintard, M.**, "Simulation of C/C composites ablation using a VOF method with moving reactive interface", *this conference* (2006).
22. **Lachaud, J., Vignoles, G. L., Goyhénèche, J.-M. and Epherre, J.-F.**, "Ablation in carbon/carbon composites : microscopic observations and 3D numerical simulation of surface roughness evolution", *Proc. 6th Pacific Rim Conf. on Ceramic and Glass Technology (PacRim6)*, to appear in *Ceram. Eng. Sci. Proc.* (2006).
23. **Vignoles, G. L.**, "Modelling Binary, Knudsen, and Transition Regime Diffusion Inside Complex Porous Media", *J. de Physique IV* **5** (1995) C5-159 – C5-166.
24. **Lachaud, J., Aspa, Y., Vignoles, G. L. and Bourget, G.**, "Experimental characterization and 3D modelling of carbon/carbon composites oxidation : role of the interface", *this conference* (2006).